

Discharge modeling in EAST using bidirectional LSTM

Chenguang Wan^{1,2,*}, Zhi Yu¹, Xiaojuan Liu¹ and Jiangan Li^{1,2,*}

1. Institute of Plasma Physics, Hefei Institutes of Physical Science, Chinese Academy of Sciences, Hefei 230031, China

2. University of Science and Technology of China, Hefei, 230026, China

E-mail: chenguang.wan@ipp.ac.cn and j_li@ipp.ac.cn

Abstract. An improved discharge model based on a bidirectional neural network was developed. The bidirectional LSTM model was used, and it was trained by the experimental data from the Experimental Advanced Superconducting Tokamak (EAST) campaign 2010-2020 discharges. Compared to our previous works (Chenguang Wan et al 2021 Nucl. Fusion **61** 066015), the present work reproduces the discharge evolution process through more key diagnostic signals, including the electron density n_e , store energy W_{mhd} , loop voltage V_{loop} , actual plasma current I_p , normalized beta β_n , toroidal beta β_t , beta poloidal β_p , elongation at plasma boundary κ , internal inductance l_i , q at magnetic axis q_0 , and q at 95% flux surface q_{95} . The similarity of electron density n_e and loop voltage V_{loop} is improved by 1%, and 5%. The average similarity of all the selected key diagnostic signals between modeling results and the experimental data are greater than 90%, except for the V_{loop} and q_0 . The model has two main application scenarios: After tokamak discharge experiment, the model gives estimated values of the diagnostic signals based on the actual actuator signals. When the actual values of the diagnostic signals are close to the estimated values it means that the discharge is normal, and vice versa it means that the discharge is abnormal or a new discharge mode occurs. Before the tokamak discharge experiment, the proposal designer sets the values of the actuator signals, and the model has the promising for giving the estimated values of the diagnostic signals to assist in checking the reasonableness of the tokamak experimental proposal.

Keywords: discharge modeling, machine learning, bidirectional LSTM Submitted to: *Nucl. Fusion*

1. Introduction

The whole discharge process modeling of tokamak is a complicated, critical and urgent problem to be solved. It is used to check the feasibility of pulse, to assist in experimental data analysis, to validate the theoretical model, to research and develop control technology, and to provide references of discharge experiment proposals [1]. However, the conventional discharge modeling from a physical point of view, the main method is "Integrated Modeling" [2] derived from first-principles. "Integrated Modeling" involves lots of different physical processes in tokamak. The accuracy of the modeling depends on the completeness and rationality of the tokamak physical process was model involved. Due to the nonlinear, multi-scale, multi-physics characteristics of tokamak, high-fidelity and faster simulation of the whole tokamak discharge process is still a great scientific challenge [3].

An alternative approach for tokamak discharge modeling without relying on integrating the complex physical model is using the neural network method. The neural networks have been employed in magnetic fusion research to solve a variety of problems, including disruption prediction [4–6], simulation acceleration [7–9], plasma tomography [10], radiated power estimation [11], identifying instabilities [12], estimating neutral beam effects [13], classifying confinement regimes [14], determination of scaling laws [15, 16], filament detection on MAST-U [17], electron temperature profile estimation via SXR with Thomson scattering [18], coil current prediction with the heat load pattern in W7-X [19], equilibrium reconstruction [18, 20–24], and equilibrium solver [25], control plasma [26–31], physic-informed machine learning [32]. Additionally, in our previous work [1], a neural-network-based method have been used on discharge modeling. In this work, only the past observation information was used without considering the future information. But offline discharge modeling differs from disruption prediction contextual information is available and equal vital for it during the experiment proposal stage. Other limitations of the previous work are only modeling three signals (electron density n_e , stored energy W_{mhd} , and loop voltage V_{loop}) which is still not enough for tokamak discharge modeling and requires the introduction of a physical model code to estimate the actual I_p as input signals. So in this paper, a new machine learning architecture was designed to consider contextual information, modeling eleven key signals of tokamak discharge, and values of all the input signals can be directly available or given by the machinelearning model without introducing physical codes.

In the present work, we trained a bidirectional LSTM model using large-scale data from EAST campaign 2010-2020 discharges. The bidirectional LSTM model can introduce contextual information in the calculation. With the 85 actuator signals input, the model is able to reproduce the whole discharge evolution process curve of eleven key diagnostic signals, including the electron density n_e , store energy W_{mhd} , loop voltage V_{loop} , actual plasma current I_p , normalized beta β_n , toroidal beta β_t , beta poloidal β_p , elongation at plasma boundary κ , internal inductance l_i , q at magnetic axis q_0 , and q at 95% flux surface q_{95} .

This paper is organized as follows. The deep learning model architectures details are given in section 2. Section 3 describes the data preprocessing and data selection criteria. The detailed model training process can be found in section 4. The experimental evaluation and comparison of previous work are given in section 5. Finally, the results are discussed and a brief conclusion is made in section 6.

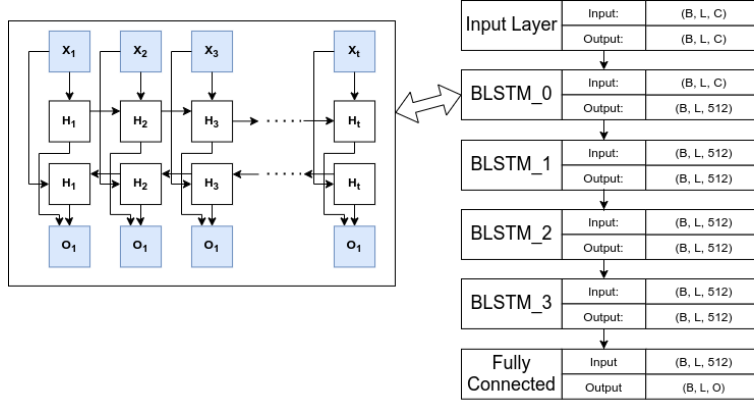


Figure 1. Architecture of bidirectional LSTM. The sub figure on the left represents a bidirectional LSTM cell. Here, B, L, C are batch size, the longest sequence length of batch, and feature size. The C is the channel number of input data, equal to 84 and 65 for modeling sycic1 and diagnostic data, respectively.

2. Model

One of the aims of this work is to improve the limitation of previous discharge modeling with machine learning. In the previous work on discharge modeling with machine learning [1], an encoder-decoder architecture was adapted, only the information before the current calculation time point was used without introducing the context information. In this work, an improved bidirectional Recurrent Neural Network (RNN) [33–35] was developed, and contextual information was taken into account. In this paper, a bidirectional LSTM cell was chosen as the fundamental cell of the bidirectional RNN.

As shown in figure 1, the deep learning model architecture based on bidirectional LSTM and stacked four bidirectional LSTMs. For any time step t , given a mini-batch input $\mathbf{X}_t \in \mathbb{R}^{n \times d}$ (number of examples: n , number of input features in each example: d) and let the hidden layer activation function be Φ . In the one layer bidirectional LSTM, we assume that the forward and backward hidden states for this time step are $\vec{\mathbf{H}}_t \in \mathbb{R}^{n \times h}$ and $\overleftarrow{\mathbf{H}}_t \in \mathbb{R}^{n \times h}$, respectively, where h is the number of hidden units. The forward and backward hidden state updates are as follows:

$$\begin{aligned} \vec{\mathbf{H}}_t &= \Phi \left(\mathbf{X}_t \mathbf{W}_{xh}^{(f)} + \vec{\mathbf{H}}_{t-1} \mathbf{W}_{hh}^{(f)} + \mathbf{b}_h^{(f)} \right), \\ \overleftarrow{\mathbf{H}}_t &= \Phi \left(\mathbf{X}_t \mathbf{W}_{xh}^{(b)} + \overleftarrow{\mathbf{H}}_{t-1} \mathbf{W}_{hh}^{(b)} + \mathbf{b}_h^{(b)} \right), \end{aligned} \quad (1)$$

where the weights $\mathbf{W}_{xh}^{(f)} \in \mathbb{R}^{d \times h}$, $\mathbf{W}_{hh}^{(f)} \in \mathbb{R}^{h \times h}$, $\mathbf{W}_{xh}^{(b)} \in \mathbb{R}^{d \times h}$, $\mathbf{W}_{hh}^{(b)} \in \mathbb{R}^{h \times h}$, and biases $\mathbf{b}_h^{(f)} \in \mathbb{R}^{1 \times h}$ and $\mathbf{b}_h^{(b)} \in \mathbb{R}^{1 \times h}$ are all the model parameters.

Next, we concatenate the forward and backward hidden states $\vec{\mathbf{H}}_t$ and $\overleftarrow{\mathbf{H}}_t$ to obtain the hidden state $\mathbf{H}_t \in \mathbb{R}^{n \times 2h}$ to be fed into the next layer.

Then again the same calculation as in equation 1. When we consider dropout, the hidden state $\mathbf{H}_t \in \mathbb{R}^{n \times 2h}$ will be randomly masked as zeros with a frequency of rate δ (in this paper, the

dropout rate is $\delta = 0.1$) at each step during *training* phase. The dropout can easily help prevent overfitting [36].

Last, the output layer computes the output $\mathbf{O}_t \in \mathbb{R}^{n \times q}$ (number of outputs: q):

$$\mathbf{O}_t = \text{activation}(\mathbf{H}_t \mathbf{W}_{hq}) + \mathbf{b}_q. \quad (2)$$

Here, the weight matrix $\mathbf{W}_{hq} \in \mathbb{R}^{2h \times q}$ and the bias $\mathbf{b}_q \in \mathbb{R}^{1 \times q}$ are the model parameters of the output layer.

One of the key features of a bidirectional LSTM is that information from both ends of the sequence is used to estimate the output. That is, we use information from *both* future and past observations to predict the current one. The activation function is a linear function not a rectified linear unit (ReLU) [37, 38] or others non-linear activation functions. Basically, for regression tasks, it is customary to use the linear function as the activation function because it's differentiable and it does not limit the output. We do not use ReLU as the activation of the last layer for this regression task due to the fact that they are limited and cannot generate all numbers which are needed.

3. Dataset

The whole EAST's data system stores more than 3000 raw channels data and thousands of processed physical analysis data [39], which record the entire process of tokamak discharge. Similar to the authors' previous paper [1], all the data of tokamak was divided into three categories: configuration parameters, actuators signals, and diagnostic signals. The discharge modeling can be essentially reduced to a process of mapping actuators (input) signals to diagnostic (output) signals.

In the present work, eleven diagnostic signals that can represent the important signals of tokamak discharge are chosen as output. The output signal includes all important 0-D EAST diagnostic signals obtained stably which are not selected by physical models or manually. This allows our model to be easily extended to other diagnostic signals that we ignored. The input signals includes all the signals that may affect the output. Detailed information about input and output signals are listed in table 1. The input signal "Ref. Shape" should be noted. According to the tokamak magnetic control system diagram [40], the "sycic1" is affected by the shape reference. So when modeling "sycic1" the shape reference data is required. Some of the table signals are processed signals with a clear physical meaning, and others are unprocessed raw acquisition signals. Since some signals of the actual EAST experimental diagnostic system are not processed, in some cases we directly selected the unprocessed raw acquisition signals. As long as the input signals contains information to determine the output, whether it is a processed physical signal will not affect the modeling result.

Tokamak discharge evolution is a complex nonlinear process, and there is no simple way to determine the connection between the actuator signals and the diagnostic signals. For different diagnostic parameters, they are determined by different inputs. In the previous work [1], the three signals W_{mhd} , n_e and V_{loop} can be directly determined by the input signals. But in the present work, the input signals can not simply and directly determine all the output signals. In our practice, l_i , β_n can not be accurately modeled by the input signals that do not include "sycic1". When the input signals includes "sycic1" all output signals of the present work can be modeled. But the "sycic1" values can not be directly obtained. In our work, the indirectly estimated values of sycic1 were given by a machine learning model.

Table 1. The list of signals. The “raw signal” means the original electrical signal and these could be converted to the signals with physical meaning.

Signals	Physics meanings	Unit	Number of Channels	Sampling rate	Meaning of Channels
Output Signals			12		
$Act.I_p$	Actual plasma current	A	1	$1kHz$	Actual plasma current
n_e	Electron density	$10^{19}m^{-3}$	1	$1kHz$	Electron density
W_{mhd}	Plasma stored energy	J	1	$20Hz$	Plasma stored energy
V_{loop}	Loop voltage	V	1	$1kHz$	Loop voltage
β_n	Normalized beta	dimensionless	1	$15Hz$	Normalized beta
β_t	Toroidal beta	dimensionless	1	$15Hz$	Toroidal beta
β_p	Beta poloidal	dimensionless	1	$15Hz$	Beta poloidal
κ	Elongation at plasma boundary	dimensionless	1	$15Hz$	Elongation at plasma boundary
l_i	Internal inductance	dimensionless	1	$15Hz$	Internal inductance
q_0	q at magnetic axis	dimensionless	1	$15Hz$	q at magnetic axis
q_{95}	q at 95% flux surface	dimensionless	1	$15Hz$	q at 95% flux surface
Feedback Signal			1		
sycic1	In-vessel coil no.1 current	A	1	$1kHz$	In-vessel coil no.1 current
Input Signals			84		
Ref. I_p	Reference plasma current	A	1	$1kHz$	Reference plasma current
PF	Current of Poloidal field (PF) coils	A	14	$1kHz$	PF 0-14 current
B_{t0}	Toroidal magnetic field	T	1	$1kHz$	Toroidal field at magnetic axis
LHW	Power of Lower Hybrid Wave Current Drive and Heating System	kW	4	$20kHz$	2.45 GHz LHW, and 4.6 GHz LHW
NBI	Neutral Beam Injection System	Raw signal	8	$5kHz$	Acceleration voltage and beam current, of No. 1-2 left/right ion source.
ICRH	Ion Cyclotron Resonance Heating System	Raw signal	16	$5kHz$	Output of detector for rejected power of No. 1-16 transmitter
ECRH/ ECCD	Electron Cyclotron Resonance Heating/Current Drive System	Raw signal	4	$50kHz$	Output of detector for injected power measurement No. 1-4 gyrotron
GPS	Gas Puffing System	Raw signal	12	$10kHz$	Horizontal ports J, K, D, B; Upper port O; Lower ports O, C, H
SMBI	Supersonic Molecular Beam Injection	Raw signal	3	$10kHz$	3 ports of SMBI
PIS	Pellet Injection System	Raw signal	1	$10kHz$	1 injection line for Pellet Injection
Ref. Shape	Shape reference	Raw signal	20	$1kHz$	11 groups of control points

4. Training

In this section, model training and data processing will be introduced in detail. The training model can be divided into four steps as follows:

- (i) Obtaining and resampling the data of 97 channels data (including input, feedback, and output signals as shown in table 1) from the EAST source database, then storing it in HDF5[‡] file with each HDF5 file data properties (standard deviation δ , mean μ , etc.) stored in MongoDB.
- (ii) Standardizing the data with z-scores (also known as standard scores) [§].
- (iii) Using bucketing batch training a deep learning model for sycic1.
- (iv) Sycic1 as input for training a deep learning model to the eleven key diagnostic signals (table 1 output signal).

4.1. Obtaining and resampling

The dataset is selected from EAST campaign 2010-2020 discharge shot number in the range #14866-88283 [41–43]. A total 26230 normal shots are selected. The normal shot means that no disruption occurred during this discharge, the flat-top lasts more than two seconds, the key signals (i.e., magnetic field, and actual plasma current I_p) are complete, at least one available model output signals. If there is not a certain magnetic field configuration, it is impossible to constrain (or control) the plasma. And it is meaningless to model the tokamak discharge without complete actual I_p . Additionally, if all the model output signals are unavailable, the deep model training or test will be impossible. Three different data sets are needed during developing the bidirectional LSTM model of discharge modeling. A training set is required for training the model. A validation set to determine which hyper-parameters of the model are best. A test set is used to measure the final accuracy of the deep learning model. The training set should use the earliest data of the selected EAST campaign to simulate the new data faced in practice. Test set and validation set are same in statistics, so that we can expect a best performance on test set by optimizing the accuracy on validation set. For each epoch, the model must input every shot in the validation set to get the performance metric, and the validation set will not update the model parameters. So relatively small validation set can accelerate the model training. The shot range of validation set and test set should not cross to ensure the objectivity of test set. The test set should only be used once at last, otherwise, there is a suspicion of looking at the answer in advance. This is one form of data leakage. These three data sets are made extremely carefully to meet these strict requirements. Shot #14866-74999 in EAST database are selected as the training set. 21192 normal shots are reserved at last. The validation set has shot numbers in the range #75000-77000. Shots #77000-88283 are the test set.

All data are resampled with the same sample rate $1kHz$. Although we used a relatively low sampling rate, the original resampled data set still contains 547GB of data. So for each shot, the data is saved to an HDF5 file, not in the database server for quick and robust training. The data properties are stored in MongoDB for double-checking the data validity and availability by the human and program.

[‡] Hierarchical Data Format (HDF) is a set of file formats (HDF4, HDF5) designed to store and organize large amounts of data.

[§] z-score is calculated by $z = (x - \mu)/\sigma$ where μ is the mean of the population. σ is the standard deviation of the population.

There are significant differences in the sampling rate of raw signals R_{raw}^i , where i is the index of signals. The input and output signal data sets need to be resampled at a common sampling rate R_c to ensure that the data points of different signals are aligned at the same time. If $R_{raw}^i < R_c$, the raw signal data needs to be linearly interpolated to complement the time series. If $R_{raw}^i > R_c$, the raw signal data needs to be down-sampled into the same sampling rate with R_c by simple moving average (SMA). In the present work, the simple moving average (SMA) calculates the average of a specific time range ($1/R_c$) of values. The SMA used the information from the later time, but the purpose of our work is to create offline modeling. Additionally, the later time information is used in bidirectional LSTM. So the later time information will not affect the use of the model. From another perspective, experimenters do not design high-frequency fluctuations in the experimental proposal stage. Filtering out high-frequency fluctuations is more appropriate for the application of the model in experimental program validation.

4.2. Standardizing

Firstly, all source data was saved in the HDF5 file. Then, discharge duration time, and every signal mean, variance, existence will save to MongoDB database shot-by-shot. Saving mean and variance of each signal of each shot data is necessary not only to double-check and scan the signal if have outliers but also for calculating the global means and standard deviations for the huge data by MapReduce. If a signal of a shot has outliers will not using in calculate the signal's global mean and standard deviation. MapReduce is a programming model and an associated implementation for processing and generating big data sets with a parallel, distributed algorithm on a cluster. The reasons for using MapReduce are large-scale data will be overflowed if calculate the global mean and standard deviation directly. When the source data means and standard deviations have been calculated, the z-scores will be applied for standardization. In this step, If the input data have NaN (invalid value) or Inf (infinite value) will be replaced by linear interpolation value and 3.2×10^{32} respectively. In statistics, the z-score is the number of standard deviations by which the value of a raw score (i.e., an observed value or data point) is above or below the mean value of what is being observed or measured. Raw scores above the mean have positive standard scores, while those below the mean have negative standard scores. z-score is calculated by $z = (x - \mu)/\sigma$ where μ is the mean of the population. σ is the standard deviation of the population.

4.3. Feedback signal.

We use a deep learning model to estimate sycic1 values. However, the input signals between modeling sycic1 and tokamak's main diagnostic signals are different. The input of modeling sycic1 deep learning model is the magnetic field coil, auxiliary heating systems, *shape reference*, etc. That is the input signals in the table 1. The shape reference is very useful for modeling sycic1 (find the reasons in details in [40]). The input signals of modeling tokamak's main diagnostic signals are using the magnetic field coil, auxiliary heating systems, *sycic1*, etc. That is, the input signals (except shape reference) and feedback signal in table 1. Sycic1 has important impacts on tokamak plasma magnetic field configuration. So when modeling the main diagnostic signals should be introduced sycic1 as input. In our practice, when the model input not includes the sycic1, the model can not modeling l_i and β_p . We should train the sycic1 model first and then train the tokamak main diagnostic signals.

4.4. Bucketing batchwise training.

Mini-batching gradient descent [44, 45] is a useful technology for improving GPU performance [46] and accelerating training convergence of deep-learning models. The gradients of the loss with respect to the parameters are computed for several examples in parallel and then averaged. For this to work efficiently, the architecture for the forward and backward pass of each gradient computation needs to be equal for all the examples computed in parallel. This is not possible if different training examples have different lengths. Thus, training RNN or its variants on a big amount of data with different length is a large and challenging problem. In the present work, the bucketing [47] was used to solve this problem.

The bucketing method can be reduce to a partition problem. Let $S = \{s_1, s_2, \dots, s_n\}$ be the set of sequences and $l_i = |s_i|$ is the length of sequence s_i . Each GPU processes sequences in a mini-batch in a synchronized parallel manner, so processing time of a mini-batch $I_{\text{batch}} = \{s_1, s_2, \dots, s_k\}$ is proportional to $O(\max_{i \in 1, \dots, k} l_i)$ and processing time of the whole set is expressed as:

$$T(S) = O(n/k * \max_{i \in 1, \dots, k} l_i) \quad (3)$$

If the sequences of the dataset were shuffled randomly before splitting the minimum and maximum sequence length in the mini-batch are very different. As the result, the GPU does additional work for processing the meaningless tails of shorter sequences. Additionally, The too-long sequence with a big batch size will be overflowed as the result of the GPU memory capacity limit. To overcome this flaw and decrease training time, we used a customized bucketing to optimize the batch training. As shown in the figure 2, we cluster all sequences to B buckets by the lengths, where $B = 3$. Let $S_i = \{s_{j_1}, s_{j_2}, \dots, s_{j_{k_i}}\}$. For every bucket we perform the mini-batch training with different batch size. The processing time of the whole set is expressed as:

$$T(S) = \sum_{i=1}^B O(T(S_i)) \quad (4)$$

In the present work, we manually partitioning the sequence length set. Because the different sequences length sets will use different batch sizes. The results of partition was shown in figure 2. The Bucket 1,2,3 is in the interval $[2, 12.3]$, $(12.3, 50]$, $(50, 412]$ respectively. Because of the GPU memory capacity limit, the batch size of the three buckets is set 8,4,1 respectively. These batch sizes can control GPU memory overflow and easily allocate the input tensor for each GPU.

The sequences within every bucket were shuffled randomly. And then the sequences were generated batch sequences batch-by-batch. To train batchwise with a batch size M , we need M independent shot discharge sequences of same bucket to feed to the GPU. The different length discharge sequences were padded by zeros to the same length. We do this by using M processes read sequence data and then zeros padding to the same length. The M sequences were fed to a buffer first to solve the problem of GPU and CPU speed mismatch to a certain extend.

4.5. The model training.

The deep learning model uses an end-to-end training that was executed on 8x Nvidia P100 GPUs with PyTorch [48] on the Centos7 operating system. The training of the deep learning model starts with weight initializer is xavier initialization [49], bias initializer is zeros, and optimizer is RMSprop [50] for solving gradient explosion. The loss function of this training should be noted. The function

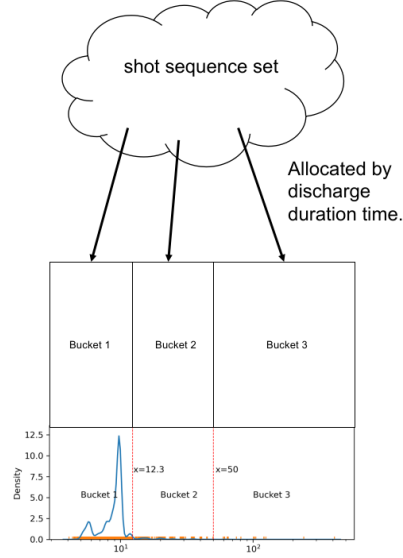


Figure 2. The length distribution of the input discharge sequences. The number of buckets $B = 3$.

is Masked MSELoss that have some improvements for mean squared error (MSE) loss function. The MaskedMSELoss can be described as:

$$l(\mathbf{x}, \mathbf{y}) = L = \frac{\sum_{i=0}^{i=N} \{l_1, l_2, \dots, l_N\}}{N}, \quad (5)$$

$$l_i = \sum_{j=0}^{j=\text{len}} (\mathbf{x}_j^i - \mathbf{y}_j^i)^2, \quad (6)$$

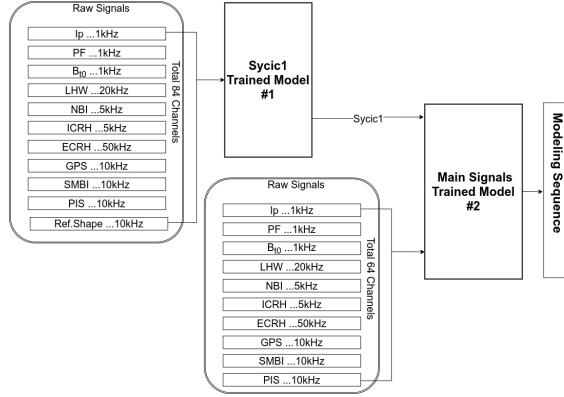
where N is the batch size, \mathbf{x} and \mathbf{y} are the batch experimental sequence and batch predicted sequence, $\mathbf{x}_j^i, \mathbf{y}_j^i$ are the j th point values of the i th experimental sequence and predicted sequence. The subtlety of this work is $j = \text{len}$, where len is the length of the i th sequence. So the masked MSE function can be prevented useless training of the zeros padding section of the sequence. The training of our model is executed several times. Many of these trials are considered as failed (e.g. divergence in training, poor performance on the test set, etc) because of unsuitable hyper-parameters. In the process of training our model, multiple sets of hyperparameters were tried. It was a trial-and-error approach on different sets of hyperparameters combinations: the best hyperparameter set was chosen on the best validation set performances. Finally, the best hyper-parameters were found and shown in table 2.

5. Results

After the deep learning model had been trained, the model can be tested on unseen data (test set). As shown in figure 3. In the present work, models are used in sequence. The #1 deep learning

Table 2. Hyperparameters in this model

Hyperparameter	Explanation	Best value
η	Learning rate	1×10^{-3}
γ	Momentum factor	0.5
L2	L2 regularization rate	0.01
Loss function	Loss function type	Maseked MSE
Optimizer	Optimization scheme	RMSprop
Dropout	Dropout probability	0.1
dt	Time step	1ms
Batch_size	Batch size	8,4,1
RNN_type	Type of RNN	Bidirectional LSTM
n_{rnn}	Number of RNN stacked	4
H_{rnn}	Hidden size of RNN	512
$n_{encoder}$	Number of BiLSTMs stacked in encoder	2
$n_{decoder}$	Number of BiLSTMs stacked in decoder	2

**Figure 3.** Using the trained model.

model is used first to get the sycic1 estimated values. And then through the #2 deep learning model to modeling the tokamak's main diagnostic signals. The preprocessing steps on new data are the same as before, keeping the training set parameters (the mean μ and the standard deviation σ) for standardization. The data whose distribution lies outside of the training set, as it was scaled with the training's standardization parameters, might affect the model's generalization capabilities. All the standardized data will be fed into the trained model and get the modeling sequence of diagnostic signals. In the final step, the corresponding model should be selected according to the diagnostic signal to be modeled.

In this section, the results of modeling will be analyzed in detail, including representative modeling results and similarity distributions. In the present work, the similarity and mean square error (MSE) are used as quantitative measurements of the modeling results accuracy and is defined

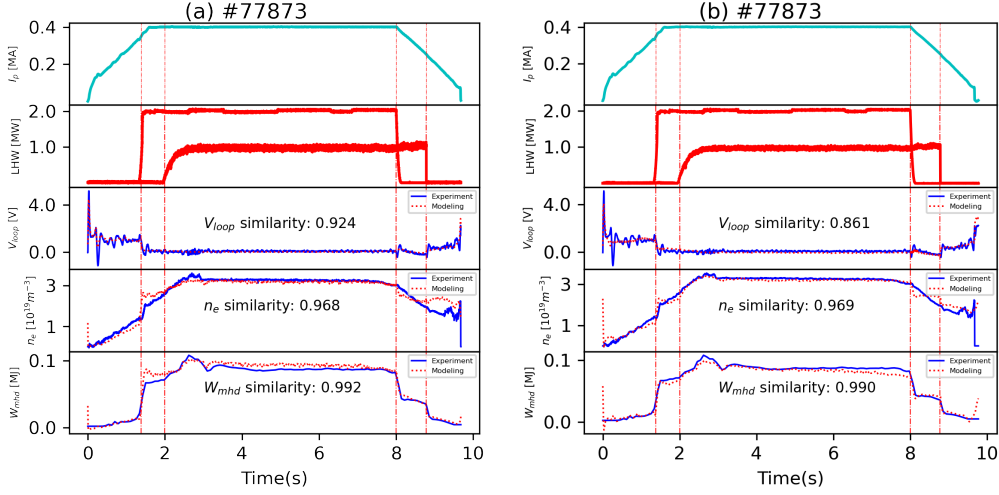


Figure 4. The comparison of the modeling results between the bidirectional LSTM (a) and encoder-decoder model (b) in a typical shot #77873.

as follows:

$$S(\mathbf{x}, \mathbf{y}) = \max\left(\frac{\Sigma(\mathbf{x} - \bar{\mathbf{x}})(\mathbf{y} - \bar{\mathbf{y}})}{\sqrt{\Sigma(\mathbf{x} - \bar{\mathbf{x}})^2 \Sigma(\mathbf{y} - \bar{\mathbf{y}})^2}}, 0\right), \quad (7)$$

$$MSE(\mathbf{x}, \mathbf{y}) = \frac{1}{n} \sum_{i=1}^n (\mathbf{x}_i - \mathbf{y}_i)^2, \quad (8)$$

where \mathbf{x} is experimental data, \mathbf{y} is modeling result, $\bar{\mathbf{x}}$, $\bar{\mathbf{y}}$ are the means of the vector \mathbf{x} and vector \mathbf{y} , x_i , y_i are the point values of the vector \mathbf{x} , \mathbf{y} . The MSE is the mean ($\frac{1}{n} \sum_{i=1}^n$) of the squares of the errors $(\mathbf{x}_i - \mathbf{y}_i)^2$. MSE will be affected by the outlier. Similarity can only measure whether the trend is consistent, but it cannot measure the difference in value.

5.1. Comparison.

In the previous work, we showed three demonstrative diagnostic signals (i.e. n_e , W_{mhd} , and V_{loop}) modeling results. In order to reasonably compare with the previous work, we test the model of the three signals modeling by the same test shot set.

As shown in figure 4, a typical EAST normal discharge shot #77873 (same as our before paper [1]) is selected to check the difference between previous and present work. Shot # 77873 has two LHW injections during discharge. Experimental data and modeling data are shown together in figure 4. The comparison shows the bidirectional LSTM can get better modeling results of V_{loop} than encoder-decoder model while not using adaptive resampling. The improvement of the modeling results in ramp-up and ramp-down phases of V_{loop} can be achieved by bidirectional LSTM modeling.

The test data set with 695 shots were used to quantitatively evaluate the improvement of the model. It is the same test set of previous work. The compared statistical results with previous work about the similarity between model results and the experimental data are shown in figure 5.

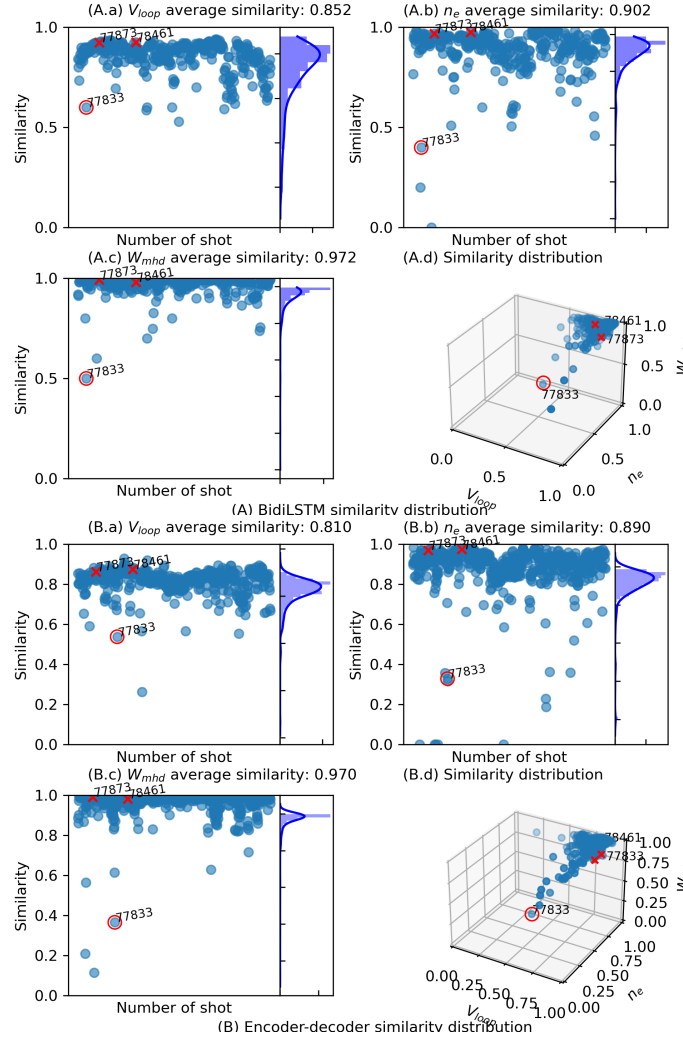


Figure 5. The comparison of similarity distribution of the same output signals (V_{loop} , n_e , and W_{mhd}) in the same test set with previous work.

Compared with the previous work, the present work has a more concentrated distribution among the three parameters (W_{mhd} , n_e and V_{loop}), whether it is for univariate or multivariable joint distribution. This feature shows that the bidirectional LSTM can better model the normal discharge shot. The bidirectional LSTM has similar outliers with previous work in the distribution, the encoder-decoder shows those points far away from the center of the cluster indicate that the experiment is running in abnormal mode [1]. The outliers have similar meanings in the bidirectional LSTM modeling results. The bidirectional LSTM has increased by $\sim 5\%$ similarity in V_{loop} modeling results while not using the adaptive resampling, and it has not improvement in W_{mhd} , the authors think the reason is W_{mhd} is good enough in the previous work. Further big improvement can not

be achieved by the bidirectional LSTM. The present model improves similarity performance of n_e by $\sim 1\%$. As shown in figure 4, the n_e bidirectional modeling result is more sensitive to changes of the external drives than encoder-decoder modeling result. This feature may be the reason why the improvement of n_e similarity performance is only 1%.

5.2. More key diagnostic signals.

As mentioned earlier, only three signals still not enough for tokamak discharge modeling and a physical model code should be involved for estimating actual I_p of input signals. In the present work, the bidirectional LSTM can reproduce the multiple diagnostic signals, from ramp-up to ramp-down without inducing a physical code. The slope of the ramp-up and the amplitude of the flat-top are accurately reproduced by the model. The model can also reflect the external auxiliary system signal impact on the diagnostic signal. As shown in figure 6, the vertical dash-dot lines indicate the rising and falling edges of the external auxiliary system signals and the plasma response. In the figure 6, we add the loss of each modeling signal for the more accurate comparison modeling and experimental signals. The MSE loss can more accurately measure the difference of values.

Whole test data set of shot range 77000-88283 is used to quantitatively evaluate the reliability of the model results of the other eight signals. The statistical results of the similarity between modeling and experiment data are shown in figure 7. Except for q_0 , the average similarity of other key signals is greater than 90%. And the similarity distribution is concentrated above 90%. The average similarity of q_0 is greater than 85%. The reason for the low average similarity of q_0 is that its value is around zero. Although the values are close, small differences will have lower similarity. The MSE loss between modeling and experiment data of q_0 is small. For example, in figure 6, the q_0 MSE loss is roughly approximately equal to q_{95} MSE loss. However, the similarity of q_0 and q_{95} are 0.764, 0.989 respectively. The similarities have relatively large difference.

All selected key diagnostic signals excluding V_{loop} can be considered to have been almost completely modeled under the normal discharge condition. As mentioned in the previous paper, Many of the V_{loop} errors are due to the plasma start-up in the ramp-up phase and the plasma shutdown in the ramp-down phase.

6. Conclusion and discussion

In previous work, we have introduced the potential that machine learning can be used to assist in experimental data analysis and proposal validation. In the present work, we show the improvement of modeling the tokamak discharge process using experimental data-driven methods. The bidirectional LSTM was developed to introduce the context information of discharge sequence to achieve a more accurate model. The model was trained on the EAST experimental dataset in shot range #14866-88283. This model can use the actuators signals to reproduce the normal discharge evolution process (i.e. electron density n_e , store energy W_{mhd} , loop voltage V_{loop} , actual plasma current I_p , normalized beta β_n , toroidal beta β_t , beta poloidal β_p , elongation at plasma boundary κ , internal inductance l_i , q at magnetic axis q_0 and q at 95% flux surface q_{95}) without additional introducing physical models. The average similarity of all the selected key diagnostic signals between modeling results and the experimental data are greater than 90%, except for the V_{loop} and q_0 . This results shows it is close to practical to use only the experimental data-driven model to assist in experimental data analysis and proposal validation.

The present work demonstrates that the experimental data-driven method can easily be

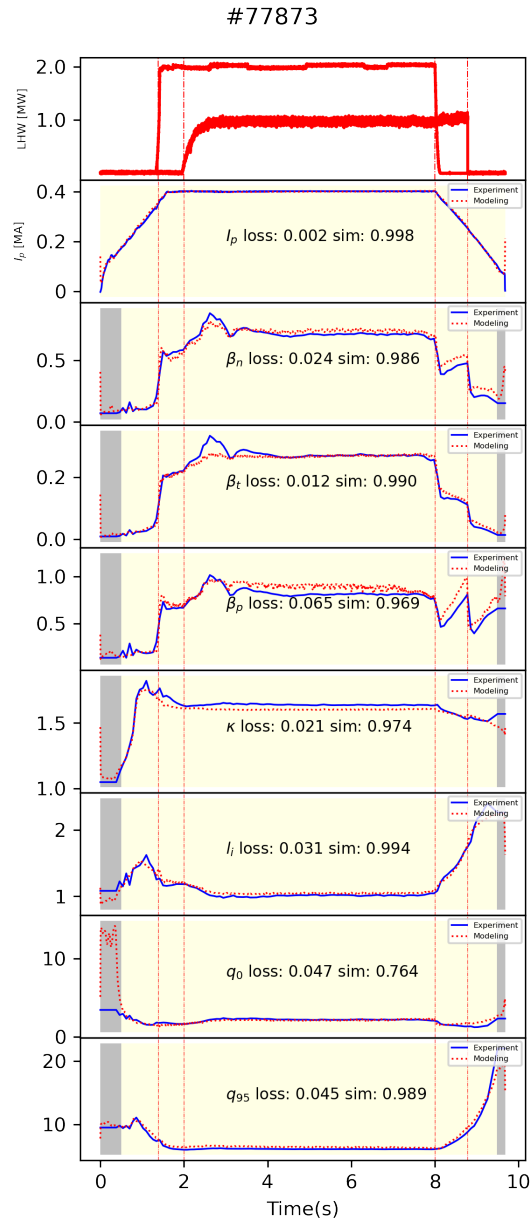


Figure 6. Comparison of the modeling result and EAST experiment data. The gray area shows no experimental data so the modeling results in the area is unreliable.

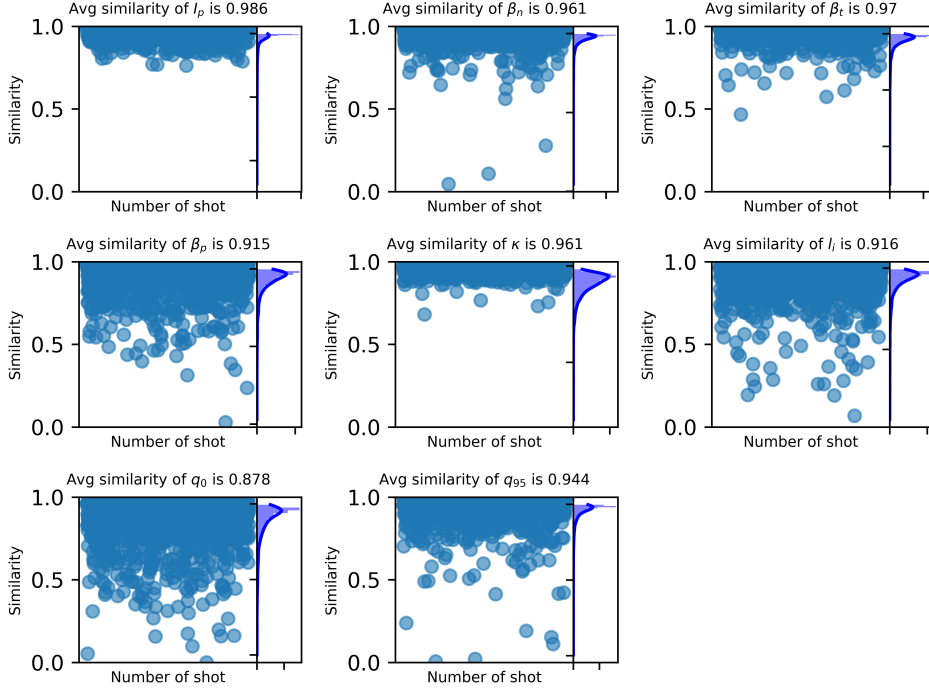


Figure 7. The similarity distribution and average similarity in the whole test set. The figure shows the similarity distributions of the output signals (see table 1) excluded W_{mhd} , n_e and V_{loop} .

extended to more diagnostic signals. Compared with physical models, experimental data-driven models have good performance on long time scales. When the machine learning model has been trained, running a trained machine learning model is taken shorter time than running a physic model for the whole process of tokamak discharge modeling. The present work shows a promising result that using experimental data-driven modeling as supplement to physical modeling tokamak. In the future work, we want to integrate the model to plasma control system (PCS) for automatically checking control strategy. Tokamak one-dimensional profiles and two-dimensional distributions are also important for tokamak discharge experiments, reconstructing them is the next step to explore.

Acknowledgments

The author would like to thank all the members of EAST Team for providing such a large quantity of past experimental data. The author Chenguang Wan sincerely thanks Qiping Yuan, Ruirui Zhang and Jinping Qian for explanation of the experimental data.

This work was supported by the National Key R&D project under Contract No.Y65GZ10593, the National MCF Energy R&D Program under Contract No.2018YFE0304100 and the Comprehensive Research Facility for Fusion Technology Program of China under Contract No. 2018-000052-73-01-001228.

References

- [1] Chenguang Wan, Zhi Yu, Feng Wang, Xiaojuan Liu, and Jiangang Li. Experiment data-driven modeling of tokamak discharge in EAST. *Nuclear Fusion*, 2021.
- [2] Gloria L. Falchetto, David Coster, Rui Coelho, B. D. Scott, Lorenzo Figini, Denis Kalupin, Eric Nardon, Silvana Nowak, Luis Lemos Alves, Jean-François F. Artaud, V. Basiuk, João P.S. Bizarro, C. Boulbe, A. Dinklage, D. Farina, B. Faugeras, J. Ferreira, A. Figueiredo, Ph Huynh, F. Imbeaux, I. Ivanova-Stanik, T. Jonsson, H. J. Klingshirn, C. Konz, A. Kus, N. B. Marushchenko, G. Pereverzev, M. Owsiak, E. Poli, Y. Peysson, R. Reimer, J. Signoret, O. Sauter, R. Stankiewicz, P. Strand, I. Voitsekhovitch, E. Westerhof, T. Zok, and W. Zwingmann. The European Integrated Tokamak Modelling (ITM) effort: Achievements and first physics results. *Nuclear Fusion*, 54(4):43018, 2014.
- [3] Paul Bonoli, Lois Curfman McInnes, C Sovinec, D Brennan, T Rognlien, P Snyder, J Candy, C Kessel, J Hittinger, and L Chacon. Report of the Workshop on Integrated Simulations for Magnetic Fusion Energy Sciences. Technical report, Massachusetts Institute of Technology, 2015.
- [4] Julian Kates-Harbeck, Alexey Svyatkovskiy, and William Tang. Predicting disruptive instabilities in controlled fusion plasmas through deep learning. *Nature*, 568(7753):526–531, apr 2019.
- [5] Wenhui Hu, Cristina Rea, Q P Yuan, Keith Erickson, Dalong Chen, Biao Shen, Yao Huang, Jianyuan Xiao, Junjie Chen, Yanmin Duan, Yang Zhang, Huidong Zhuang, Jichan Xu, Kevin Joseph Montes, Robert Granetz, Long Zeng, Jinping Qian, Bingjia Xiao, and Jiangang Li. Real-time prediction of high density EAST disruptions using Random Forest. *Nuclear Fusion*, 2021.
- [6] Bihao Guo, Dalong Chen, Biao Shen, Cristina Rea, Robert Granetz, Long Zeng, Wenhui Hu, Jinping Qian, Youwen Sun, and Bingjia Xiao. Disruption prediction on EAST tokamak using a deep learning algorithm. *Plasma Physics and Controlled Fusion*, aug 2021.
- [7] M. Honda and E. Narita. Machine-learning assisted steady-state profile predictions using global optimization techniques. *Physics of Plasmas*, 26(10), 2019.
- [8] O Meneghini, S P Smith, P B Snyder, G M Staebler, J Candy, E Belli, L Lao, M Kostuk, T Luce, T Luda, J M Park, and F Poli. Self-consistent core-pedestal transport simulations with neural network accelerated models. *Nuclear Fusion*, 57(8):86034, jul 2017.
- [9] O Meneghini, G Snoep, B C Lyons, J McClenaghan, C S Imai, B Grierson, S P Smith, G M Staebler, P B Snyder, J Candy, E Belli, L Lao, J M Park, J Citrin, T L Cordemiglia, A Tema, and S Mordijck. Neural-network accelerated coupled core-pedestal simulations with self-consistent transport of impurities and compatible with {ITER} {IMAS}. *Nuclear Fusion*, 61(2):26006, dec 2020.
- [10] Diogo R Ferreira, Pedro J Carvalho, and J E T Contributors. Deep Learning for Plasma Tomography in Nuclear Fusion. pages 1–5, 2020.
- [11] O Barana, A Murari, P Franz, L C Ingesson, and G Manduchi. Neural networks for real time determination of radiated power in JET. *Review of scientific instruments*, 73(5):2038–2043, 2002.
- [12] A Murari, P Arena, A Buscarino, L Fortuna, and M Iachello. On the identification of instabilities with neural networks on JET. *Nuclear Instruments and Methods in Physics*

- Research Section A: Accelerators, Spectrometers, Detectors and Associated Equipment*, 720:2–6, 2013.
- [13] M D Boyer, S Kaye, and K Erickson. Real-time capable modeling of neutral beam injection on {NSTX}-U using neural networks. *Nuclear Fusion*, 59(5):56008, mar 2019.
- [14] A Murari, D Mazon, N Martin, G Vagliasindi, and M Gelfusa. Exploratory Data Analysis Techniques to Determine the Dimensionality of Complex Nonlinear Phenomena: The L-to-H Transition at JET as a Case Study. *IEEE Transactions on Plasma Science*, 40(5):1386–1394, may 2012.
- [15] A Murari, J Vega, D Mazon, D Patané, G Vagliasindi, P Arena, N Martin, N F Martin, G Rattá, and V Caloone. Machine learning for the identification of scaling laws and dynamical systems directly from data in fusion. *Nuclear Instruments and Methods in Physics Research Section A: Accelerators, Spectrometers, Detectors and Associated Equipment*, 623(2):850–854, 2010.
- [16] P Gaudio, A Murari, M Gelfusa, I Lupelli, and J Vega. An alternative approach to the determination of scaling law expressions for the L-to-H transition in Tokamaks utilizing classification tools instead of regression. *Plasma Physics and Controlled Fusion*, 56(11):114002, oct 2014.
- [17] B Cannas, S Carcangiu, A Fanni, T Farley, F Militello, A Montisci, F Pisano, G Sias, and N Walkden. Towards an automatic filament detector with a Faster R-CNN on MAST-U. *Fusion Engineering and Design*, 146:374–377, 2019.
- [18] D. J. Clayton, K. Tritz, D. Stutman, R. E. Bell, A. Diallo, B P LeBlanc, and M. Podestà. Electron temperature profile reconstructions from multi-energy SXR measurements using neural networks. *Plasma Physics and Controlled Fusion*, 55(9):095015, sep 2013.
- [19] Daniel Böckenhoff, Marko Blatzheim, Hauke Hölbe, Holger Niemann, Fabio Pisano, Roger Labahn, and Thomas Sunn Pedersen. Reconstruction of magnetic configurations in W7-X using artificial neural networks. *Nuclear Fusion*, 58(5):56009, mar 2018.
- [20] E Coccoresse, C Morabito, and Raffaele Martone. Identification of noncircular plasma equilibria using a neural network approach. *Nuclear Fusion*, 34(10):1349, 1994.
- [21] Chris M Bishop, Paul S Haynes, Mike E U Smith, Tom N Todd, and David L Trotman. Fast feedback control of a high temperature fusion plasma. *Neural Computing & Applications*, 2(3):148–159, 1994.
- [22] Young-Mu Jeon, Yong-Su Na, Myung-Rak Kim, and Y S Hwang. Newly developed double neural network concept for reliable fast plasma position control. *Review of Scientific Instruments*, 72(1):513–516, 2001.
- [23] S. Y. Wang, Z. Y. Chen, D. W. Huang, R. H. Tong, W. Yan, Y. N. Wei, T. K. Ma, M. Zhang, G. Zhuang, Huang D W Tong R H Yan W Wei Y N Ma T K Zhang M Wang S Y Chen Z Y, Zhuang G, S. Y. Wang, Z. Y. Chen, D. W. Huang, R. H. Tong, W. Yan, Y. N. Wei, T. K. Ma, M. Zhang, and G. Zhuang. Prediction of density limit disruptions on the j-TEXT tokamak. *Plasma Physics and Controlled Fusion*, 58(5), apr 2016.
- [24] Semin Joung, Jaewook Kim, Sehyun Kwak, J G Bak, S G Lee, H S Han, H S Kim, Geunho Lee, Daeho Kwon, and Y.-C. Ghim. Deep neural network Grad-to-Shafranov solver constrained with measured magnetic signals. *Nuclear Fusion*, 60(1):16034, dec 2019.
- [25] B Ph. van Milligen, V Tribaldos, and J A Jiménez. Neural Network Differential Equation and Plasma Equilibrium Solver. *Phys. Rev. Lett.*, 75(20):3594–3597, nov 1995.

- [26] Chris M Bishop, Paul S Haynes, Mike E U Smith, Tom N Todd, and David L Trotman. Real-time control of a tokamak plasma using neural networks. *Neural Computation*, 7(1):206–217, 1995.
- [27] Bin Yang, Zhenxing Liu, Xianmin Song, and Xiangwen Li. Design of {HL}-2A plasma position predictive model based on deep learning. *Plasma Physics and Controlled Fusion*, 62(12):125022, nov 2020.
- [28] T Wakatsuki, T Suzuki, N Hayashi, N Oyama, and S Ide. Safety factor profile control with reduced central solenoid flux consumption during plasma current ramp-up phase using a reinforcement learning technique. *Nuclear Fusion*, 59(6), may 2019.
- [29] H. Rasouli, C. Rasouli, and A. Koochi. Identification and control of plasma vertical position using neural network in Damavand tokamak. *Review of Scientific Instruments*, 84(2), 2013.
- [30] Bin Yang, Zhenxing Liu, Xianmin Song, Xiangwen Li, and Yan Li. Modeling of the HL-2A plasma vertical displacement control system based on deep learning and its controller design. *Plasma Physics and Controlled Fusion*, 62(7):75004, jul 2020.
- [31] Jaemin Seo, Y.-S. Na, B. Kim, C.Y. Lee, M.S. Park, S.J. Park, and Y.H. Lee. Feedforward beta control in the KSTAR tokamak by deep reinforcement learning. *Nuclear Fusion*, 61(10):106010, oct 2021.
- [32] George Em Karniadakis, Ioannis G. Kevrekidis, Lu Lu, Paris Perdikaris, Sifan Wang, and Liu Yang. Physics-informed machine learning. *Nature Reviews Physics*, 3(6):422–440, jun 2021.
- [33] Trias Thireou and Martin Reczko. Bidirectional long short-term memory networks for predicting the subcellular localization of eukaryotic proteins. *IEEE/ACM Transactions on Computational Biology and Bioinformatics*, 4(3):441–446, 2007.
- [34] Mike Schuster and Kuldeep K Paliwal. Bidirectional recurrent neural networks. *IEEE transactions on Signal Processing*, 45(11):2673–2681, 1997.
- [35] Alex Graves and Jürgen Schmidhuber. Framewise phoneme classification with bidirectional LSTM and other neural network architectures. *Neural Networks*, 18(5-6):602–610, 2005.
- [36] Nitish Srivastava, Geoffrey Hinton, Alex Krizhevsky, Ilya Sutskever, and Ruslan Salakhutdinov. Dropout: A simple way to prevent neural networks from overfitting. *Journal of Machine Learning Research*, 15(1):1929–1958, 2014.
- [37] Richard H R Hahnloser, H Sebastian Seung, and Jean-Jacques Slotine. Permitted and forbidden sets in symmetric threshold-linear networks. *Neural computation*, 15(3):621–638, 2003.
- [38] Richard H. R. Hahnloser, Rahul Sarpeshkar, Misha A. Mahowald, Rodney J. Douglas, and H. Sebastian Seung. Digital selection and analogue amplification coexist in a cortex-inspired silicon circuit. *Nature*, 405(6789):947–951, jun 2000.
- [39] Feng Wang, Yueting Wang, Ying Chen, Shi Li, and Fei Yang. Study of web-based management for EAST MDSplus data system. *Fusion Engineering and Design*, 129(June 2017):88–93, apr 2018.
- [40] Gianmaria De Tommasi. Plasma Magnetic Control in Tokamak Devices. *Journal of Fusion Energy*, 38(3-4):406–436, aug 2019.
- [41] Baonian Wan, Jiangang Li, Houyang Guo, Yunfeng Liang, Guosheng Xu, Liang Wang, and Xianzu Gong. Advances in H-mode physics for long-pulse operation on {EAST}. *Nuclear Fusion*, 55(10):104015, jul 2015.

- [42] Baonian Wan, Jiangang Li, Houyang Guo, Yunfeng Liang, Guosheng Xu, and Xianzhu Gong. Progress of long pulse and H-mode experiments in EAST. *Nuclear Fusion*, 53(10), 2013.
- [43] Jiangang Li, Baonian Wan, EAST Team, and Int Collaborators. Recent progress in RF heating and long-pulse experiments on EAST. *Nuclear Fusion*, 51(9, SI), sep 2011.
- [44] Jeffrey Dean, Greg S Corrado, Rajat Monga, Kai Chen, Matthieu Devin, Quoc V Le, Mark Z Mao, Marc'Aurelio Marc'aurelio Ranzato, Andrew Senior, Paul Tucker, Others, and Ke Yang. Large scale distributed deep networks. *Advances in neural information processing systems*, pages 1223–1231, 2012.
- [45] Zhiheng Huang, Geoffrey Zweig, Michael Levit, Benoit Dumoulin, Barlas Oguz, and Shawn Chang. Accelerating recurrent neural network training via two stage classes and parallelization. In *2013 IEEE Workshop on Automatic Speech Recognition and Understanding*, pages 326–331. IEEE, dec 2013.
- [46] Sharan Chetlur, Cliff Woolley, Philippe Vandermersch, Jonathan Cohen, John Tran, Bryan Catanzaro, and Evan Shelhamer. cuDNN: Efficient Primitives for Deep Learning. oct 2014.
- [47] Viacheslav Khomenko, Oleg Shyshkov, Olga Radyvonenko, and Kostiantyn Bokhan. Accelerating recurrent neural network training using sequence bucketing and multi-GPU data parallelization. In *2016 IEEE First International Conference on Data Stream Mining & Processing (DSMP)*, pages 100–103. IEEE, aug 2016.
- [48] Adam Paszke, Sam Gross, Francisco Massa, Adam Lerer, James Bradbury, Gregory Chanan, Trevor Killeen, Zeming Lin, Natalia Gimelshein, Luca Antiga, Alban Desmaison, Andreas Kopf, Edward Yang, Zachary DeVito, Martin Raison, Alykhan Tejani, Sasank Chilamkurthy, Benoit Steiner, Lu Fang, Junjie Bai, and Soumith Chintala. PyTorch: An Imperative Style, High-Performance Deep Learning Library. In H Wallach, H Larochelle, A Beygelzimer, F d\textquotesingle Alché-Buc, E Fox, and R Garnett, editors, *Advances in Neural Information Processing Systems 32*, pages 8024–8035. Curran Associates, Inc., 2019.
- [49] Xavier Glorot and Yoshua Bengio. Understanding the difficulty of training deep feedforward neural networks. In *Journal of Machine Learning Research*, volume 9, pages 249–256, 2010.
- [50] Alex Graves. Generating Sequences With Recurrent Neural Networks. *arXiv preprint arXiv:1308.0850*, aug 2013.